

# Comparing autonomous low cost sensors with terrestrial lidar for monitoring spring phenology

Tom Schenkels

September 17, 2014



WAGENINGEN UNIVERSITY  
WAGENINGEN UR





# Comparing autonomous low cost sensors with terrestrial lidar for monitoring spring phenology

Tom Schenkels

Registration number 900827735080

Supervisors:

Kim Calders  
Jan Verbesselt

A thesis submitted in partial fulfilment of the degree of Master of Science  
at Wageningen University and Research Centre,  
The Netherlands.

17-9-2014  
Wageningen, The Netherlands

Thesis code number: GRS-80436

Thesis Report:                   GIRS-2014-33  
Wageningen University and Research Centre  
Laboratory of Geo-Information Science and Remote Sensing



## Abstract

Autonomous low cost instruments like PASTIS57 could deliver temporally and spatially dense datasets on regional phenology. In this research PASTIS57 is compared with terrestrial laser scanning (TLS) for spring phenology monitoring. A dataset with a high temporal resolution is gathered in a temperate broadleaf forest in The Netherlands in spring 2014. Data processing methods are designed for optimal plant area index (PAI) derivation from PASTIS57 data. We compare PAI derived from PASTIS57 and TLS measurements. We fit logistic models to PAI time series to derive descriptive variables. Start of season dates derived from PASTIS57 measurements are compared with start of season dates derived from TLS, field observations and meteorology data. We implement a processing method for PASTIS57 data which removes cloud-influenced measurements (lowering CV(RMSE) of model fitting with  $> 2\%$ ). PAI measurements from PASTIS57 instruments show similar trends as TLS measurements. Difference in measured spring PAI increase is smaller than 0.54. PAI during the leaf-off periods and leaf-on periods is measured lower by PASTIS57 by  $0.8 \pm 0.2$  and  $0.4 \pm 0.4$ . Start of season dates derived from PASTIS57 are later than TLS for three plots (by 2, 6 and 8 days) and earlier by 5 days for the fourth plot. Compared to field observations, PASTIS57 is earlier for that same plot by 8 days and later for the other plots by 1, 6 and 6 days. These results show PASTIS57 to be a cost-effective method for large-scale phenology monitoring. With more research focusing on the methods to employ these instruments, they could prove valuable for global phenology monitoring.

**Keywords:** spring phenology monitoring, autonomous low cost instruments, PASTIS57, terrestrial lidar, TLS

## **Acknowledgements**

Foremost, I would like to express my gratitude to my supervisors ir. Kim Calders and dr.ir. Jan Verbesselt for the invaluable ideas, support and feedback that they provided on my thesis. Next to my advisors I also wish to thank prof. dr. Martin Herold for taking part in my thesis examination. Thanks also to dr. Frédéric Baret for advice regarding the PASTIS57 instruments. Also thanks to dr. Harm Bartholomeus, Alvaro Lau and Philip Wenting for their assistance during field measurements and to ir. Mathieu Decuyper for his thoughts on the ecological aspects of this research. I also thank Kimberley Opie, dr. Allard de Wit and Masih Rajaei Najafabadi for their assistance on the hemispherical photography.

I thank my housemates Melissa, Jorien, Johan and Kenny for their support and distraction throughout the whole process. Also thanks to Dieteke and Kees for reviewing my thesis.

# Contents

<b>1. Introduction</b>	<b>5</b>
<b>2. Study Area and Data Collection</b>	<b>7</b>
2.1. Study area . . . . .	7
2.2. Sensor data . . . . .	7
2.2.1. PASTIS57 . . . . .	8
2.2.2. Terrestrial lidar . . . . .	10
2.3. Meteorological data . . . . .	10
2.4. Phenology field observations . . . . .	10
<b>3. Methods</b>	<b>12</b>
3.1. Sensor data processing . . . . .	12
3.1.1. PASTIS57 . . . . .	12
3.1.2. Terrestrial lidar . . . . .	13
3.2. Fitting logistic models to PAI time series . . . . .	14
3.3. Deriving start of season . . . . .	14
3.4. Instrument intercomparison . . . . .	16
<b>4. Results</b>	<b>17</b>
4.1. PASTIS57 PAI processing . . . . .	17
4.2. PAI time series . . . . .	17
4.3. Deriving start of season . . . . .	21
<b>5. Discussion</b>	<b>23</b>
<b>6. Conclusion</b>	<b>26</b>
<b>A. Fieldwork Guidelines Dassenbos 2014</b>	<b>31</b>
<b>B. Hemispherical photography</b>	<b>33</b>
B.1. Introduction . . . . .	33
B.2. Methods . . . . .	33
B.3. Results . . . . .	34
B.4. Discussion . . . . .	34
<b>C. R script listings</b>	<b>35</b>



# 1. Introduction

Forests are of global importance because of the ecological and economical services they provide. An increasing topic of interest is the dynamics of carbon stocks (Herold and Skutsch, 2011, De Sy et al., 2012). Accurate information on forest structure and its biophysical variables is essential for research on forests. Knowledge on forest vegetation density is important for modeling evapotranspiration, photosynthesis and carbon and nutrient cycles (Waring and Running, 2010).

The structure of a forest is often represented using the plant area index (PAI). This index is defined as the single-sided plant surface area per unit ground surface area. It includes the surface of both foliage and woody elements. That is why we use the term PAI instead of the commonly used term leaf area index, which name implies that only foliage surfaces are considered. Plant area volume density (PAVD) profiles are the derivative of PAI over height. They describe the distribution of plant density along the vertical dimension. PAVD profiles are used to investigate vertical forest structure. Most passive remote sensing systems are unable to provide these profiles. Destructive harvesting, leaf-litter traps and digital hemispherical photography have been used to estimate plot-level PAI (Rich, 1990, Jonckheere et al., 2004). Terrestrial lidar scanning (TLS) has recently come into focus as a method for estimating local PAI and PAVD profiles (Jupp et al., 2009).

Leaf development during spring is an important process in deciduous forests. Research on *spring phenology* is important for ecological research and global warming research. Specific interest goes out to the start of season (SOS) variable. This indicates the day of the year when leaves start to emerge. This event is easily measured and is influenced by relatively few factors unlike events that take place in summer or fall. It is a variable used in indicating shifting phenological cycles under the influence of climate change. To investigate phenological variables like these, extensive PAI measurements are needed. However, PAI data with a high temporal detail of leaf-development during spring is only limitedly available in literature (Bequet et al., 2011, Eitel et al., 2013). Phenological studies relate the timing of budburst (when leaves emerge from their buds) in temperate forests to temperature (Melaas et al., 2013, Vitasse et al., 2009, Karlsen et al., 2007, Black et al., 2000), growing degree-days (Von Wuehlich et al., 1996) and temperature extremes and radiation levels (Bequet et al., 2011). Different models are used to estimate SOS, these vary in methodology and results (Botta et al., 2000, Richardson and Keefe, 2009). Budburst takes place earlier for understory species so they can benefit from spring light levels before the canopy closes up (Richardson and Keefe, 2009, Gond et al., 1999). Ryu et al. (2014) have shown that the onset of greenness in MODIS NDVI data is determined by understory canopy development. Active systems (Culvenor, 2012, Eitel et al., 2013, Jupp et al., 2009) and some passive systems (Ryu et al., 2014) provide PAVD

profiles. These can aid understanding of air- and spaceborn remote sensing greenness products.

Most terrestrial active and passive instruments for forest structure assessment require manual operation. This limits the temporal resolution of datasets that can be acquired. Recently, low cost systems that can measure PAI autonomously at high temporal resolutions were developed. Amongst these are active systems as presented in [Culvenor \(2012\)](#), [Eitel et al. \(2013\)](#). These are powered by solar panels and actively transmit their measurements to the internet. They deliver datasets with a temporal resolution of a day or less. Using active lidar ranging, these instruments can deliver PAVD profiles. Another system, PASTIS57, uses passive sensors to measure transmittance ([Baret et al., 2010](#), [Simic et al., 2012](#)). It saves data locally and lasts 8 months on one battery charge. At a cost of €200 (Jan Verbesselt, personal communication, September 5, 2014) these instruments can be applied in large-scale phenology monitoring campaigns. Literature on PASTIS57 does not provide validation.

Large-scale phenology data would be valuable for ecological and global warming related research. That is why we focus on a new type of instrument for acquiring such data.

The objectives of this research are:

**RQ1:** How to optimize PASTIS57 data processing for monitoring PAI?

**RQ2:** How do PAI values measured with the PASTIS57 instrument compare to PAI values derived from TLS?

**RQ3:** How do start of season dates from PASTIS57 compare to TLS, meteorology and field observation start of season dates?

We will acquire a temporally dense TLS dataset with multiple scans per week throughout the spring season. Throughout the season data will also be acquired with PASTIS57 instruments. We will validate the PASTIS57 instrument for the purpose of measuring spring phenology. SOS derived from both instruments will be compared to meteorological and field observation derived SOS.

## 2. Study Area and Data Collection

### 2.1. Study area

The *Dassenbos* study area (51.9829° N, 5.6557° E) is a pedunculate oak (*Quercus robur*) dominated forest with a small presence of birch trees (*Betula spp.*) in the upper canopy. The forest is about 40 years old and is located on flat terrain.

Plot	A	B	C	D
Canopy closure	Closed	Intermediate	Intermediate	Open
Canopy composition	85% <i>Quercus robur</i> , 15% <i>Betula spp.</i>	85% <i>Quercus robur</i> , 15% <i>Betula spp.</i>	95% <i>Quercus robur</i> , 5% <i>Betula spp.</i>	97% <i>Quercus robur</i> , 3% <i>Betula spp.</i>
Understory composition	Dense with all understory species present close (2m) to the plot center.	Medium, all understory species present but at 5m from plot center.	Open, some <i>S. nigra</i> individuals present 4m from plot center.	Open, two <i>S. nigra</i> individuals close to each other at 2.5m from plot center.
Ground layer composition	70% <i>Rubus spp.</i> , 30% unpopulated	50% <i>Rubus spp.</i> , 50% <i>Lonicera spp.</i>	85% <i>Rubus spp.</i> , 15% <i>Lonicera spp.</i>	100% <i>Rubus spp.</i>

Table 2.1.: Canopy, understory and ground layer characteristics of the studied plots

Four plots were established within the forest. These were chosen for their varying canopy closure and different composition of undergrowth. Characteristics of the plots are described in Tab. 2.1. Hemispherical photographs taken with a Nikon D7000 camera with a Sigma 4.5mm lens are shown in Fig. 2.1. A map of the study area with the field plots and the locations of the meteorology stations used is shown in Fig. 2.2.

### 2.2. Sensor data

For this study data was collected with a terrestrial lidar scanner and with low cost autonomous PASTIS57 instruments (Baret et al., 2010). Six PASTIS57 instruments were installed on February 27th and measured throughout the spring season. Only for day of year (DOY) 175-176 and DOY 183 is unavailable. On the first days the instruments had to be removed temporarily. On DOY 183 the internal clock of the instruments were set to a wrong timezone. Terrestrial laser scanning (TLS) data was gathered on 48 days. From DOY 55 until DOY 136 three measurements were gathered each week on monday,

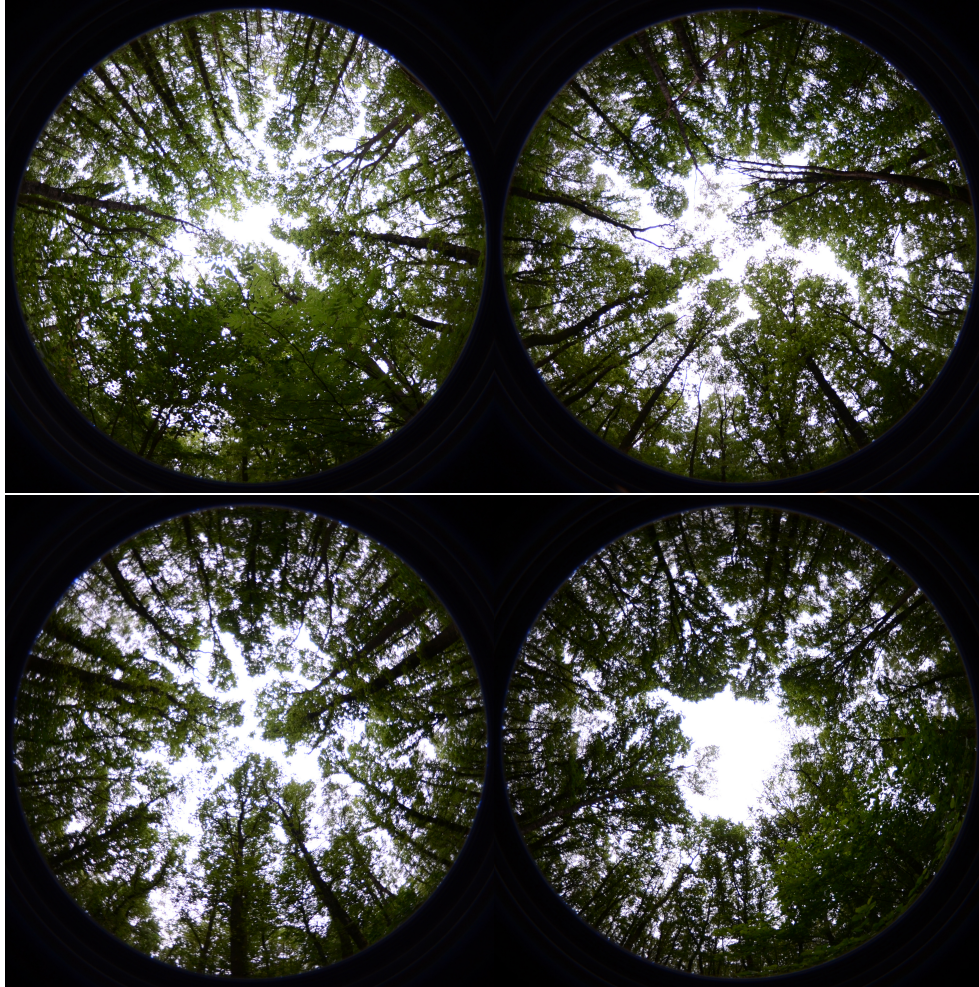


Figure 2.1.: Hemispherical photographs of plots A-D made on May 23rd using a Nikon D7000 camera and Sigma 4.5mm F2.8 lens.

wednesday and friday. On monday April 14th (DOY 104) data could not be gathered due to persistent bad weather conditions. Data was gathered on tuesday, wednesday and friday that week instead. From DOY 139 to 164 data was gathered two times per week for four weeks until DOY 164. Then once a week for four weeks until DOY 191.

### 2.2.1. PASTIS57

Six PASTIS57 instruments were used to measure incoming radiation at a 5-minute interval. Each instrument has six LED based sensors with a  $22^{\circ}$  zenith field-of-view (Baret et al., 2010). The ratio between measured irradiance at instruments in and outside the forest is used to calculate transmittance and PAI. Four instruments were placed at plots A, B, C and D. Two instruments were placed outside the forest to capture all incoming radiation (one serving as backup). All instruments were mounted on 1.3m high posts.



Figure 2.2.: Maps showing location of study area and meteorology stations and plot locations.

	PASTIS57	TLS
Data	6 measurements at 57.5° zenith	point cloud
Time required	-	20 minutes/plot fieldwork, 2 minutes/scan
Influenced by	-	wet foliage, rain, wind
Approximate price	€200 (Jan Verbesselt, personal communication, September 5, 2014)	€50,000 - €150,000 (Newnham et al., 2012)

Table 2.2.: Comparison of the PASTIS57 and TLS instruments

### 2.2.2. Terrestrial lidar

Terrestrial lidar data was gathered using a RIEGL VZ-400 3D terrestrial scanner (RIEGL Laser Measurement Systems GmbH). The instrument has a scan resolution of 0.35 mrad. It emits an infrared laser beam and can measure up to 350 m. The instrument records up to four returns per emitted light pulse.

For each measurement the TLS is positioned on a tripod at a height of approximately 1.45m. The laser viewpoint is oriented East. Minimum range is set to 0.5m and scan resolution to 0.06°. The scanner has a zenith field-of-view of 30° to 130°. Therefore two combined scans are required to capture the full hemisphere. Reflectors are placed North and South of the scanner in order to combine the scans together. A 360° scan is made in upright position and a subsequent scan in 90° tilted position.

### 2.3. Meteorological data

Hourly sunshine and hourly temperature data were available from the nearby *Veenkampen* meteorology station (51.9808°N, 5.6217°E) going back to 2012. Hourly mean temperature was measured at 1.5 m height. Hourly mean temperatures were averaged for each day to calculate the daily mean temperature (WMO, 2011). Data from 2001 to 2011 was acquired from the *Haarweg* meteorology station (51.9707°N, 5.6426°E). The location of the meteorology stations is shown in Fig. 2.2.

### 2.4. Phenology field observations

During the field campaign, leaf-setting notes have been recorded on visually apparent changes. Budburst of canopy oak and birch trees as well as the understory vegetation was described. These observations were always done by the same person to maintain objectivity.



Figure 2.3.: PASTIS57 instrument during the field campaign. The front cover is removed and the six sensors are mounted on top oriented to different azimuth angles.

## 3. Methods

### 3.1. Sensor data processing

PASTIS57 and TLS data were processed to provide comparable PAI time series. For PASTIS57, daily PAI estimates are derived. For TLS PAI is derived per measurement which amounts to 1 to 3 times per week.

#### 3.1.1. PASTIS57

Per instrument we only 4 out of 6 sensors could be used. This was because the orientation of the six sensors varied between instruments placed inside and outside the forest. For plots A, C and D, the used sensors were oriented to 0, 135, 180 and 315° azimuth, for plot B the used sensors were oriented to 0, 45, 180 and 225° azimuth (with North being 0° azimuth). Instruments measured every 5 minutes. Measurements were not synchronized between instruments. This was corrected for by changing the time of each measurement to the nearest whole 5 minutes. Data from DOY 176, 176 and 183 was excluded, for the first two days the instruments outside the forest had to be removed. On the third day the internal clock of the instruments was set to a wrong timezone. Measurements where one of four values exceeded 4000 were removed because sensors saturate at that value.

To derive PAI values, the Beer-Lambert equation (Eq. 3.1) (Baret et al., 2010) is used.  $G(z)$  is the projection function describing light transmittance for different leaf angle distributions. For the *hinge* angle (57.5° zenith), this function is approximately 0.5 regardless of leaf angle distribution (Jupp et al., 2009). Apparent transmittance  $Po(z)$  is acquired by dividing the signal  $s_i$  of the instrument located in the forest by the signal of the instrument located outside the forest  $s_o$ . Eq. 3.2 is used to calculate PAI.

$$PAI = -\frac{\cos(57.5^\circ)}{G(57.5^\circ)} \log(Po(57.5^\circ)) \quad (3.1)$$

$$PAI = -1.075 \log\left(\frac{s_i}{s_o}\right) \quad (3.2)$$

We average four values measured by instruments located in and outside the forest. We then apply Eq. 3.2 once on those two averages. This gives a single PAI estimate for each plot for every 5 minutes. Infinite and negative PAI estimates are removed. Fig. 3.1 shows PAI estimations for three subsequent days. This data shows occasional large spread of estimates. To minimize the influence of outliers the median is used as the PAI estimate for that day (the implementation of this processing step can be found in App. C in *processP57.R*).

Fig. 3.1 shows similar patterns for plots A, C and D on each of the three days. Data for plot B is not shown because the patterns were different because the sensors were



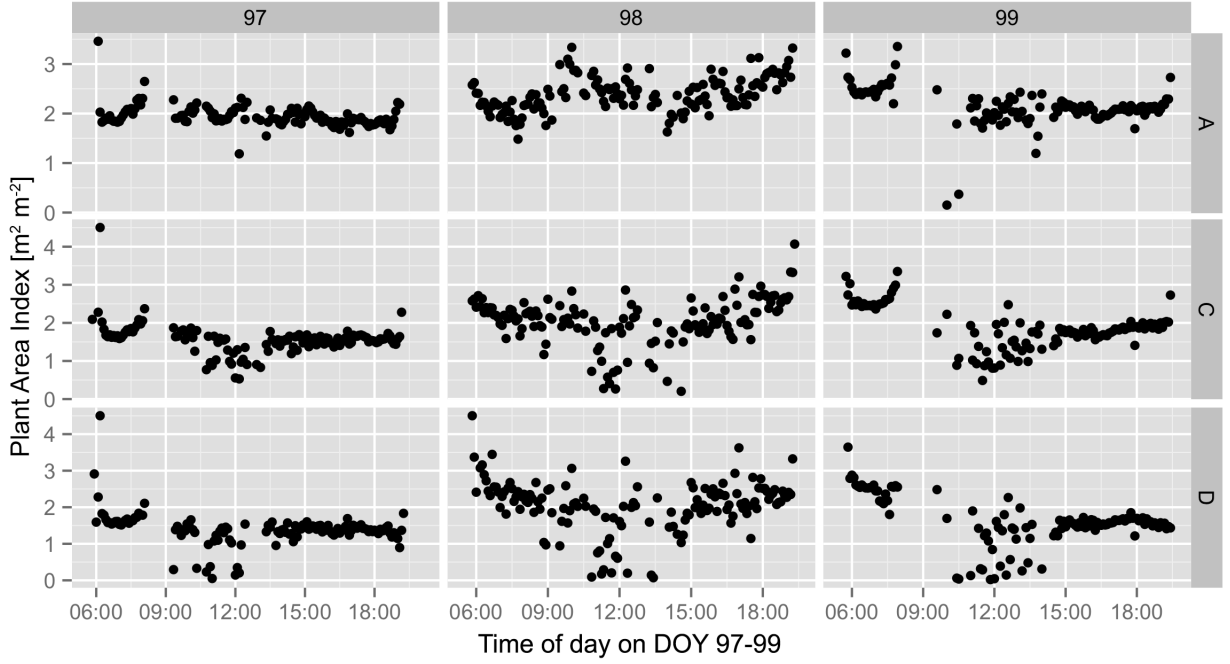


Figure 3.1.: PAI values for three days for plots A, C and D derived from PASTIS57 data

oriented different. For plots A, C and D PAI on DOY 98 is estimated higher because all PAI estimates for that day are higher. PAI values for DOY 98 show a large spread throughout the day. This indicates that an external factor influences PAI calculations for all instruments. Cloud cover and the changing diffuse and direct light conditions associated with it are a major factor causing spread of PAI estimations. Hourly sunshine duration data was available from the *Veenkampen* meteorology station. This data was used to remove data for days when less than 4 hours of sunshine was recorded (the implementation of this processing step can be found in App. C in *filterP57.R*).

### 3.1.2. Terrestrial lidar

Per measurement, the upright and tilted scans are combined using the measured reflector positions. Local topography is corrected by fitting a surface to returns classified as ground returns.

$P_{gap}(\theta, z)$  is used for deriving PAI from point cloud data (Calders et al., 2014a,b) (Eq.3.3).  $P_{gap}(\theta, z)$  gives the probability of a pulse not hitting any vegetation below height  $z$ . It calculates this for a laser pulse emitted in a zenith range around zenith angle  $\theta$ . The numerator gives the number of returns measured. If  $n_s$  returns are measured for a laser pulse, each return represents a value of  $n_s^{-1}$ .

$$P_{gap}(\theta, z) = 1 - \frac{\sum w_i(z_i < z, \theta)}{N(\theta)} \quad (3.3)$$

$$w = 1/n_s$$

$Pgap(\theta, z)$  is then used to derive PAI using a solid-angle-weighted normalized profile Jupp et al. (2009).

### 3.2. Fitting logistic models to PAI time series

In order to compare different instruments, descriptive variables are needed on which PAI time series can be compared. In this study, we will derive these variables by fitting logistic growth models to PAI time series. These models have commonly been used to describe growth in ecology (Che et al., 2014). Eq. 3.4 shows the logistic model. Fitting the model to a PAI time series gives estimates of  $L$ ,  $U$ ,  $k$  and  $t_m$  variables. These indicate the lower and upper PAI asymptote, growth rate and the inflection point (the implementation of this process can be found in App. C in *sigmoids.R*).

$$y(t) = \frac{U - L}{1 + e^{(-k(t-t_m))}} + L \quad (3.4)$$

The acquired variables will be used to describe characteristics of the leaf-off, leaf-setting and leaf-on phenology periods.

### 3.3. Deriving start of season

Start of season (SOS) describes the DOY that leaves start to emerge for deciduous species. It is a good indicator of shifting growing seasons. We used logistic models fitted to PAI measurements to derive SOS. We define SOS as the moment when the PAI value inferred from the logistic model exceeds the upper limit of the 95% prediction interval of the lower asymptote  $L$  (Che et al., 2014). Fig. 3.2 illustrates this method for the filtered PASTIS57 data of plot A (the model exceeds 1.60 on DOY 83).

SOS was derived from meteorological data according to a method described in Jeong et al. (2012), Chiang and Brown (2007). This model implements a *chilling requirement* besides mean temperature as a driving factor for budburst. This requirement models the fact that cold days in winter induce growth in spring time. In the model, mean temperature is accumulated in a *growing degree days* variable ( $GDD$ ). This is the sum of daily average temperatures ( $T$ ) exceeding a threshold  $T_h$  from the start of a year:

$$GDD(t) = \sum_{Jan1}^t \max(T - T_{th}, 0) \quad (3.5)$$

For  $T_{th}$  we used a value of 5°C (Bequet et al., 2011, Jeong et al., 2012, Botta et al., 2000).

The number of chill days  $NCD_{(t)}$  is calculated as the number of days since November 1 of the previous year for which daily mean temperature  $T$  was below  $T_{th}$ . SOS is then defined as the day when

$$GDD(t) \geq a + be^{cNCD(t)} \quad (3.6)$$

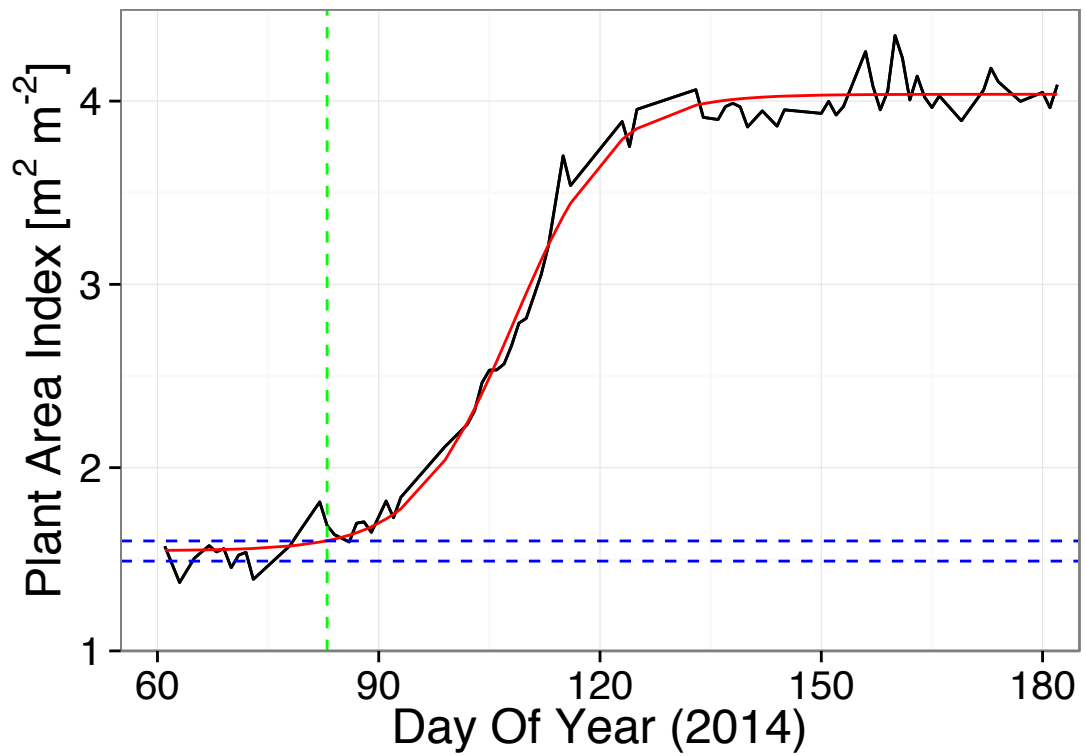


Figure 3.2.: Illustration of SOS derivation. The black solid line represents filtered PASTIS57 PAI estimates. The red solid line represents the logistic model fitted to the data. The blue dashed lines represent upper and lower limits of the 95% confidence interval of the lower asymptote  $L$ . The green dashed line represents the derived SOS DOY 83, when the PAI of the model surpasses the upper limit of the confidence interval.

For  $a$ ,  $b$  and  $c$  we used values  $a = -68$ ,  $b = 638$  and  $c = -0.010$ , which were approximated in [Botta et al. \(2000\)](#) for cool deciduous broadleaf forests ( $r^2 = 0.59$ ) (the implementation of this process can be found in App. C in *01runModel.R*).

### 3.4. Instrument intercomparison

During the field campaign no ground truth PAI values were gathered. Direct methods like usage of litter traps during the autumn leaf-fall period or destructive sampling can be used ([Cutini et al., 1998](#)). We will use TLS data as ground truth during this study. TLS data has been validated for PAI derivation [Calders et al. \(2014a,b\)](#). We will compare PASTIS57 derived PAI time series with TLS derived PAI time series.

PAI estimates acquired should be stable over the leaf-off period since only woody biomass is present in this period. Stability of measurements in the leaf-off phase is evaluated by the size of the prediction interval of the lower asymptote.

Variables derived from model fitting are used for comparing time series. Absolute PAI values of the upper and lower asymptotes as well as relative PAI increase derived from PASTIS57 and TLS are compared. PASTIS57 SOS is compared with leaf phenology field observations and TLS and meteorology derived SOS.

## 4. Results

### 4.1. PASTIS57 PAI processing

Unfiltered daily derived PAI values from PASTIS57 measurements are shown in the top panel of Fig. 4.1. PAI changes with a maximum of 0.1 for most days. On several days however, PAI is about 0.5 higher at all plots compared to the days prior and after. This is visible on DOY 98, 119 and 147-149. Days with steady lower values surround these days with higher PAI measurements (DOY 96-105, 120-125 and 137-154).

These sudden increases were assumed to be caused by clouds causing irregular irradiation. PAI estimates were removed from the time series depending on the duration of sunlight measured on a day. Registered sunshine hours and the filtered PAI time series are shown in the middle and bottom panel of Fig. 4.1. Most PAI increases mentioned before are now removed, although some remain around DOY 154-160. Out of 123 PAI estimates, 53 were removed leaving 70 PAI estimates. At the end of the leaf-setting period data is removed for six (DOY 117-122) and seven (DOY 126-132) subsequent days.

Model fitting results (Tab. 4.1) show an improved fit on the filtered data. CV(RMSE) is reduced by 2, 2.4, 2 and 1.4 percent for plots A, B, C and D respectively. Confidence intervals decreased in size by 0.03, 0.01, 0.02 and -0.02 for the  $L$  asymptote and by 0.02, 0.01, 0.02 and -0.01 for the  $U$  asymptote.

### 4.2. PAI time series

The third panel of Fig. 4.1 shows filtered PAI measurements from the PASTIS57 instruments. The S-curve with increasing PAI is visible in the data. All plots have a PAI of  $1.4 \pm 0.2$  during the leaf-off period from DOY 58 to 90. Then the PAI increases sharply for all plots. The PAI at plot A is consistently higher than the PAI at other plots during the leaf-setting period. Plot B and C increase up to 3.8 to reach a similar PAI as plot A. PAI for plot D ends up lower at about 3.6.

Fig. 4.2 shows PAI measurements derived from the TLS instrument. The S-curve with increasing PAI is visible in the TLS data. All plots show a stable PAI of  $2.1 \pm 0.1$  for DOY 55-90. PAI increases until DOY 120 when PAI increase stops and the leaf-on plateau is reached. Plot B reaches the highest PAI at about 4.8, plot D ends up at about 4.6 and plot A and C reach about 4.2. Around DOY 128 PAI of all plots decreases by 0.1 to 0.2. PAI values for all plots continue to increase with about 0.3.

Parameter results of fitting logistic models to the different PAI time series are shown in Tab. 4.1. Differences between PASTIS57 and TLS derived PAI measurements can be identified from these variables. Lower asymptotes  $L$  representing PAI levels during leaf-off periods shows that PAI estimated using PASTIS57 is  $0.8 \pm 0.2$  lower than TLS derived PAI during the leaf-off period. Upper asymptotes  $U$  representing PAI levels during leaf-

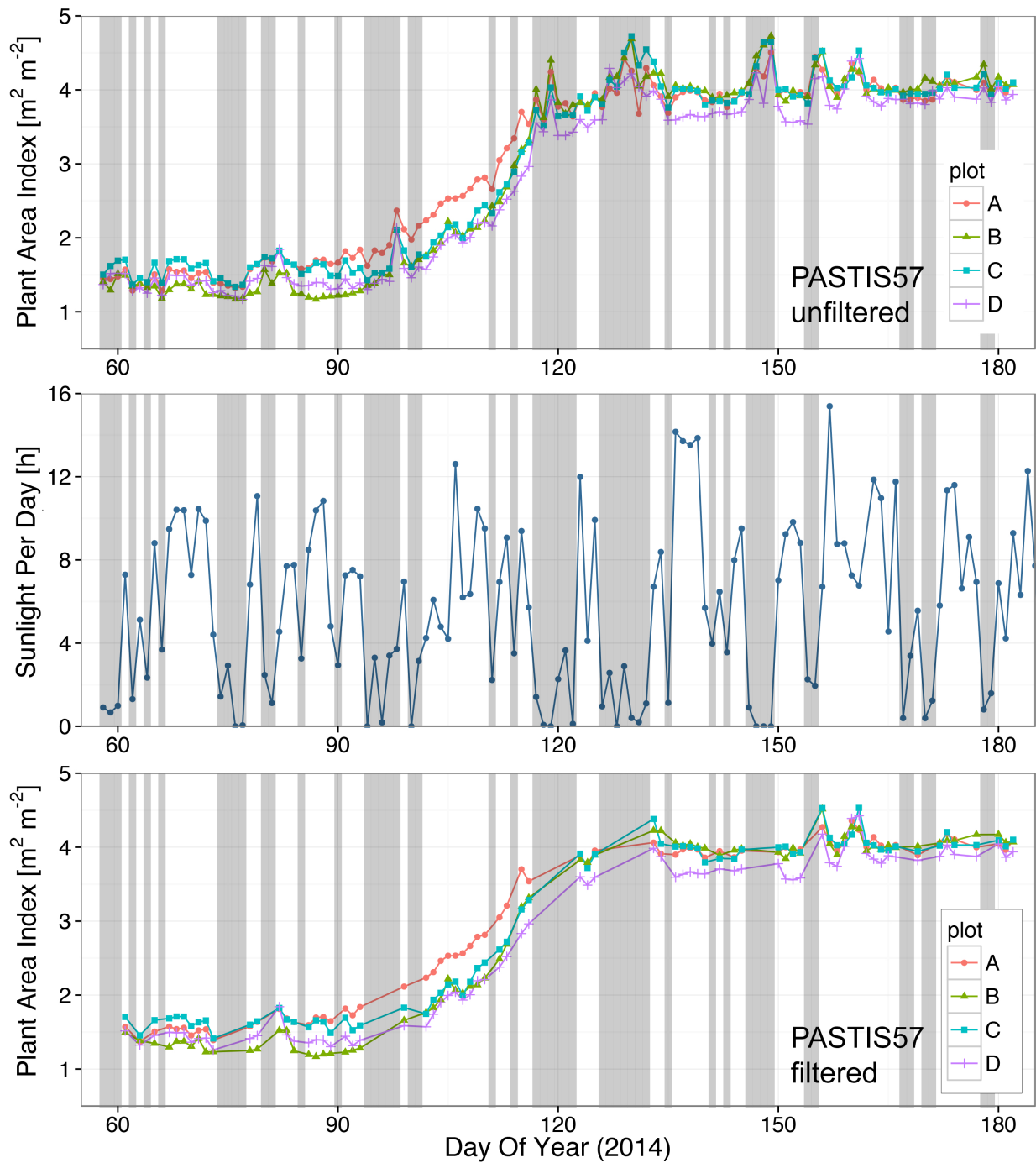


Figure 4.1.: PASTIS57 PAI measurements and filtering results. Top panel: unfiltered daily PAI values for all plots derived from PASTIS57 measurements. Middle panel: hours of sunshine per day measured at Veenkampen meteorology station. Bottom panel: filtered PAI time series from PASTIS57 measurements. Grey rectangles indicate days that were filtered.

Plot	Data	CV(RMSE)	$L$	$U$	$k$	$t_m[DOY]$	$SOS_{mod}$ [DOY]
A	P57	5.3	1.50 (1.43; 1.57)	4.05 (4.00; 4.10)	0.16 (0.14; 0.18)	108 (106.79; 108.81)	85
	P57f	3.3	1.55 (1.49; 1.60)	4.04 (4.00; 4.08)	0.15 (0.13; 0.17)	109 (107.47; 109.07)	83
	TLS	1.5	2.22 (2.19; 2.24)	4.17(4.14; 4.20)	0.18(0.17; 0.20)	111 (110.1; 111.3)	88
B	P57	6.9	1.34 (1.27; 1.40)	4.12 (4.07; 4.17)	0.22 (0.19; 0.26)	112 (110.72; 112.45)	95
	P57f	4.5	1.31 (1.25; 1.37)	4.07 (4.02; 4.11)	0.19 (0.16; 0.22)	112 (111.27; 112.89)	92
	TLS	1.7	2.29 (2.25; 2.32)	4.89 (4.86; 4.93)	0.20 (0.19; 0.22)	110 (109.9; 110.9)	90
C	P57	6.4	1.58 (1.52; 1.65)	4.09 (4.04; 4.15)	0.24 (0.20; 0.29)	113 (111.83; 113.62)	98
	P57f	4.4	1.63 (1.57; 1.68)	4.05 (4.01; 4.10)	0.21 (0.18; 0.26)	113 (112.20; 113.95)	99
	TLS	1.6	2.10 (2.07; 2.12)	4.08 (4.05; 4.10)	0.21 (0.19; 0.24)	113 (112.1; 113.0)	93
D	P57	7.2	1.41 (1.34; 1.47)	3.89 (3.83; 3.94)	0.22 (0.18; 0.27)	113 (111.86; 113.81)	97
	P57f	5.8	1.41 (1.34; 1.49)	3.86 (3.80; 3.92)	0.18 (0.14; 0.22)	114 (112.36; 114.84)	99
	TLS	2.4	2.23 (2.19; 2.27)	4.59 (4.55; 4.63)	0.18 (0.16; 0.21)	113 (112.6; 114.0)	91

Table 4.1.: Parameters of the fitted logistic growth models. P57 represents PASTIS57 data, P57f represents filtered PASTIS57 data.  $SOS_{mod}$  gives the SOS DOY derived from the fitted model. Values in parentheses indicate the lower and upper limit of 95% confidence intervals.

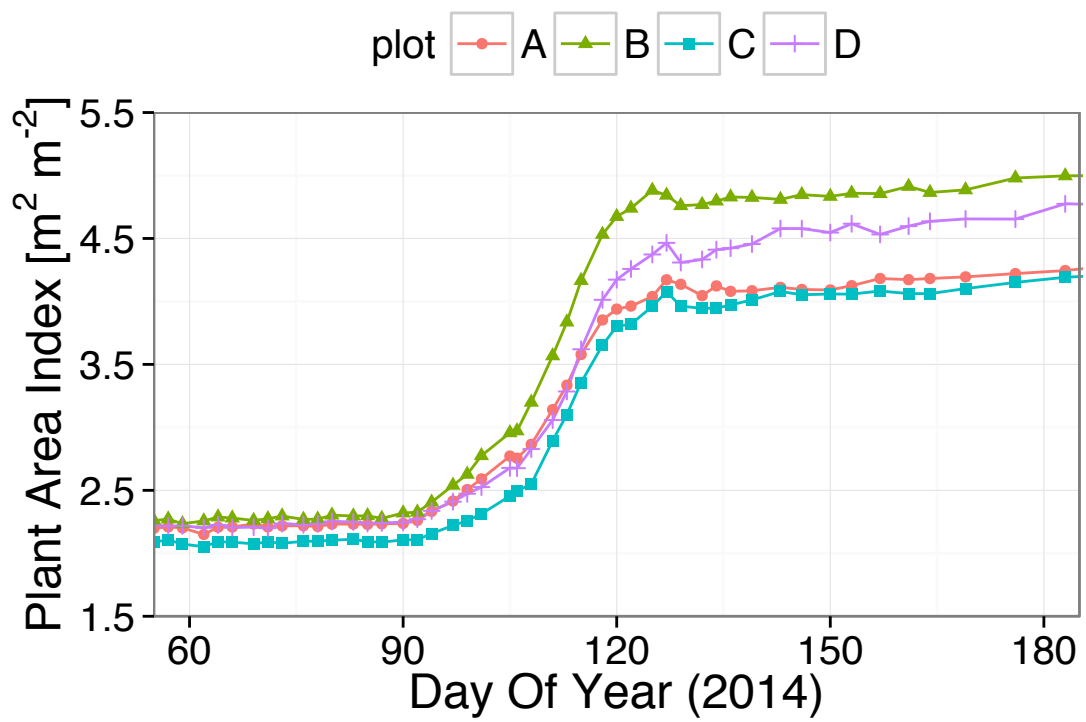


Figure 4.2.: PAI values for all plots derived from TLS measurements



on periods show that PAI estimated by PASTIS57 is  $0.4 \pm 0.4$  lower than TLS in leaf-on period. PAI increase ( $U - L$ ) reveals increases of 2.49, 2.76, 2.42 and 2.45 for PASTIS57 and 1.95, 2.60, 1.98 and 2.36 for TLS for plots A, B, C and D respectively. Confidence intervals for the lower asymptote  $L$  show that PASTIS57 measurements are less stable than TLS during leaf-off period; the confidence interval is about 0.13 as compared to 0.03 for TLS. Fig. 4.3 shows PAI measurements derived from filtered PASTIS57 and TLS data for plot A.

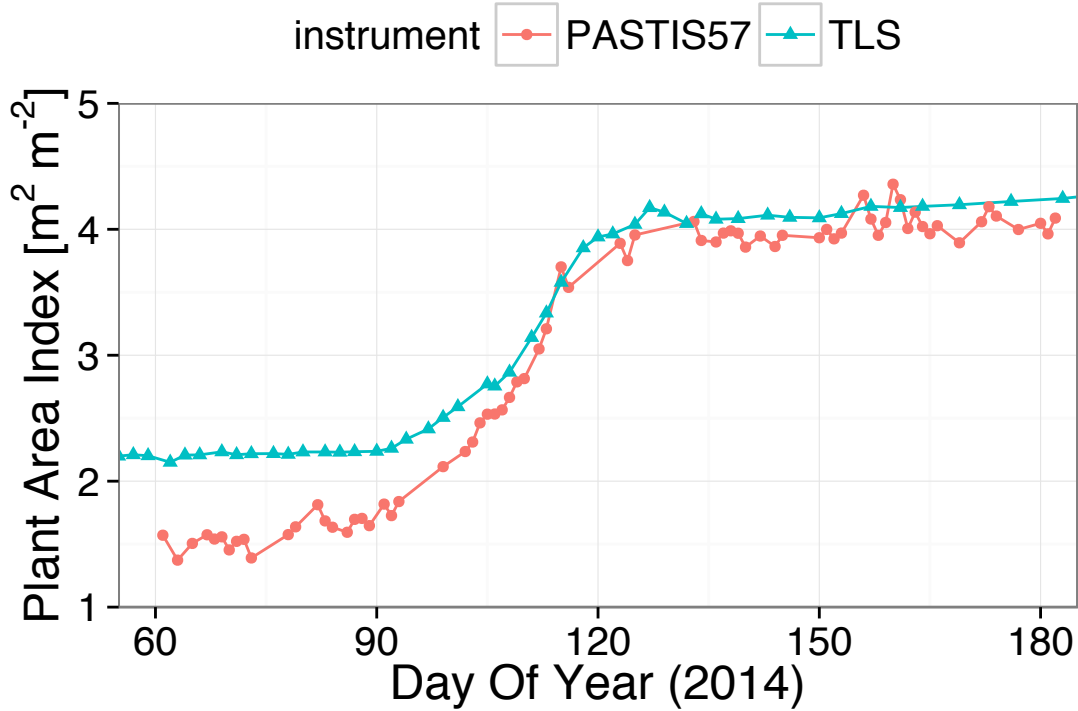


Figure 4.3.: PAI values for plot A derived from PASTIS57 and TLS measurements

### 4.3. Deriving start of season

SOS was derived from the fitted logistic models for PASTIS57 and TLS measurements. Resulting SOS DOY are shown in the  $SOS_{mod}$  column in Tab. 4.1. SOS DOY for PASTIS57 are 83, 92, 99 and 99 for plots A to D respectively. SOS estimates are combined in Tab 4.2.

Compared to TLS derived SOS, PASTIS57 is 5 days earlier for plot A and 2, 6 and 8 days later for plots B, C and D respectively.

Field observations indicate SOS between DOY 90-92 for birch trees and DOY 93-94 for oak trees. Plots A and B have about 15% birch trees (Tab. 2.1), so measuring an earlier SOS at those plots is more likely. We will thus assume SOS to be 91 for plots A and B

and 93 for plots C and D. Compared to these, PASTIS57 derived SOS is about 8 days early for plot A, one day late at plot B and 5 days late for plots C and D. The model predicting SOS for 2014 from meteorological data is illustrated in Fig. The resulting SOS is 115, this is more than 16 days later than the PASTIS57 derived SOS estimates for all plots.

Plot	PASTIS57	TLS	field observations	meteorological data
A	83	88	$\pm 91$	115
B	92	90	$\pm 91$	115
C	99	93	$\pm 93$	115
D	99	91	$\pm 93$	115

Table 4.2.: SOS estimates (in DOY) for all plots estimated from four different sources of data.

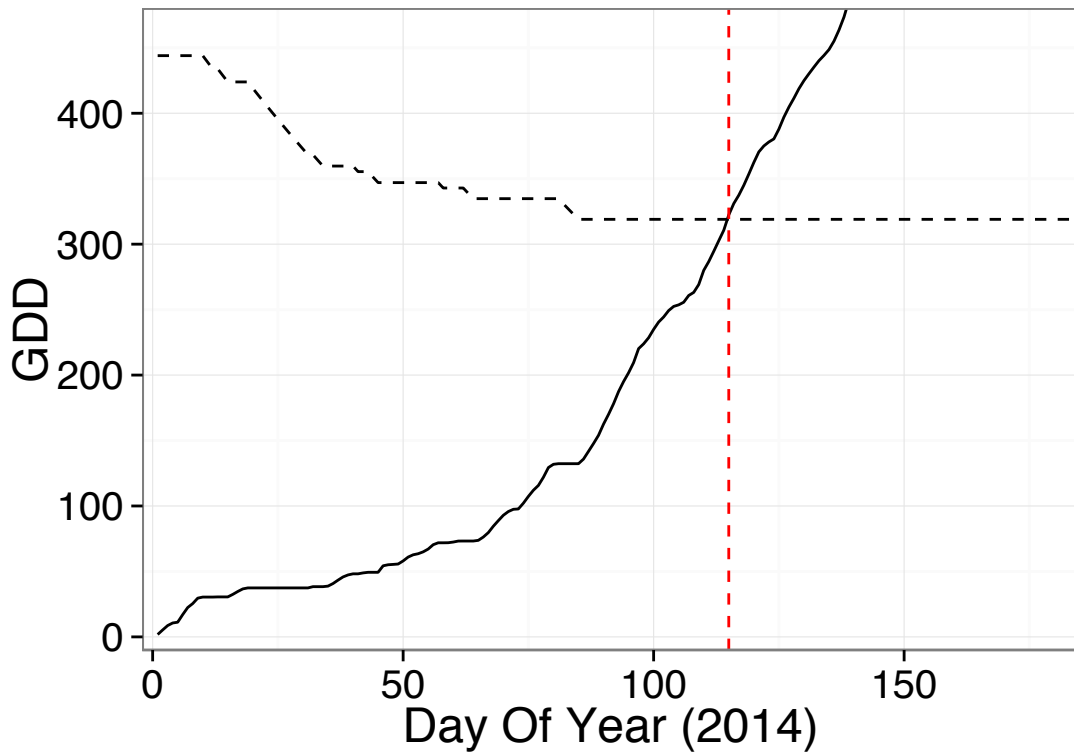


Figure 4.4.: Graph showing derivation of SOS using the NCD-GDD model. The black solid line represents cumulative  $GDD$  from January 1. The black dashed line represents the right side of Eq. 3.6 incorporating  $NCD$ . The red dashed line represents the derived SOS.

## 5. Discussion

The first objective of this research was to optimize PASTIS57 data processing for monitoring PAI. Results of initial data processing showed sudden PAI increases. *Dr. Frédéric Baret* (personal communication) raised some possible explanations: sunlight could be scattered into a sensor indirectly; sunlight could reach instruments in- and outside of the forest at uneven times; low light conditions could lead to division of two very small numbers causing extreme PAI estimates. A filtering technique was applied which removed the PAI estimate for a day if sunshine duration was less than 4 hours. This method lowered CV(RMSE) from 5.3%-7.2% to 3.3%-5.8%.

This data processing method can be improved. It removes many data points and it can not guarantee that remaining data is not influenced by clouds. Also, the threshold of 4 sunlight hours ignores the changing amount of sunlight hours throughout the year. Filtering could be improved by assessing cloud presence on a smaller time interval. Available meteorology data provides sunshine duration values for hourly and ten minute time intervals. These values could be used to identify when clouds might have influenced measurements. Data gathered before, during and after these periods could be ignored when deriving PAI. Periods with either constant sunshine or no sunshine can safely be used for PAI derivation. These indicate clear skies and constant cloud cover, conditions in which valid PAI measurements can be derived. When the sun is near the horizon signal values are low due to low irradiance levels. Dividing such small numbers for PAI estimation can lead to wrong extreme PAI estimates and should thus be avoided.

PASTIS57 measurement stability was improved by filtering but is still less than TLS measurement stability. One reason for this is the difference in resolution of the two instruments. A TLS based PAI estimate is derived from more data points than a PASTIS57 estimate.

Improvements to PASTIS57 derived estimates can also be achieved by sampling design. Position and orientation of sensors can optimize measurements. [Baret et al. \(2010\)](#) explain how they orient all six sensors North to reduce direct irradiation effects. It has to be investigated in future work which sampling design produces the best results.

The second objective of this research was to compare PASTIS57 PAI measurements to TLS PAI measurements. It was found that PASTIS57 derived PAI estimates were  $0.8 \pm 0.2$  lower during leaf-off and  $0.4 \pm 0.4$  lower during the leaf-on period. PAI increase measured using PASTIS57 was higher by 0.1-0.5. PAI estimates from TLS measurements are more stable (model fitting confidence interval of  $\pm 0.10$  for PASTIS57 versus  $\pm 0.03$  for TLS).

Whether TLS or PASTIS57 values better approximate ground truth PAI values can not be determined with remote sensing instruments. [Lovell et al. \(2012\)](#) argue that passive systems will underestimate PAI while active systems overestimate PAI. The reason would

be that passive systems measure the amount of dark vegetation on a light sky. Light scattering and diffraction will increase the apparent size of canopy gaps. Active systems measure vegetation density by recording the return of a finite light beam. This will lead to a dilation of the size of objects measured and thus to an overestimation of PAI. We therefore recommend direct methods like litter traps during autumn leaf-fall period or destructive sampling to calibrate PASTIS57 for accurate PAI estimates (Cutini et al., 1998)).

Hemispherical photography was also acquired but not used due to flawed results, a discussion on this is found in App. B.

The third objective of this research was to compare PASTIS57 start of season dates with start of season dates derived from TLS, meteorology and field observation data. We found that PASTIS57 derived start of season (SOS) shows higher variance than TLS, field observation and meteorology derived SOS.

Only plot A PASTIS57 SOS is earlier than TLS SOS (by 5 days). This is caused by masking of TLS data of the plot. A branch was located within the 0.5 m minimum range of the TLS causing it to be registered by the device as a canopy gap. This led to high  $P_{gap}$  values and thus to a low PAI estimate (Calders et al., 2014a). In some scans, the branch would be registered in the 55 to 60° zenith range. Due to the scaling of PAI on this zenith range, estimates were even lower for these scans. Therefore the 115 to 245° azimuth range of TLS scans at plot A was masked. However, the branch was part of a shrub that initiated growth as one of the first plants at plot A (DOY 76). Due to the masking of this data in TLS data, this early growth was not registered by TLS. PASTIS57 estimates did include this shrub in SOS estimates, that is why PASTIS57 measurements estimated earlier SOS plot A.

Compared to the other three TLS estimates PASTIS57 SOS estimates might be later because of the limited field-of-view of the sensors. This is limited to the hinge angle zenith range and a limited azimuth range. TLS SOS estimates are different because the full hemisphere is captured in scans. This makes that different parts of the vegetation are used for SOS derivation.

Meteorology derived SOS dates are very late compared to all other estimates. Analysis of meteorology data of previous years showed this season had the second highest GDD and second lowest NCD (see Fig. 5.1). These extreme values led to an SOS that could not be derived from the model. Driving factors like mean temperature and chilling days during winter seem to have more complex influences than what is included in the model. Models like the GDD-NCD can not be relied upon for SOS estimation.

$SOS_{mod}$  as shown in Tab. 4.1 was calculated for TLS, unfiltered and filtered PASTIS57 data with the same method. This causes two problems. Firstly, the arbitrarily chosen size of the confidence interval influences derived SOS. Choosing a bigger confidence interval leads to a later SOS prediction. Therefore this method needs to be calibrated to ground truth data to get correct SOS estimates.

A second problem is that the size of the confidence interval is dependent on the number of measurements in the time series. Thus a dataset with less measurements will lead to a later SOS estimate because the confidence interval is larger.

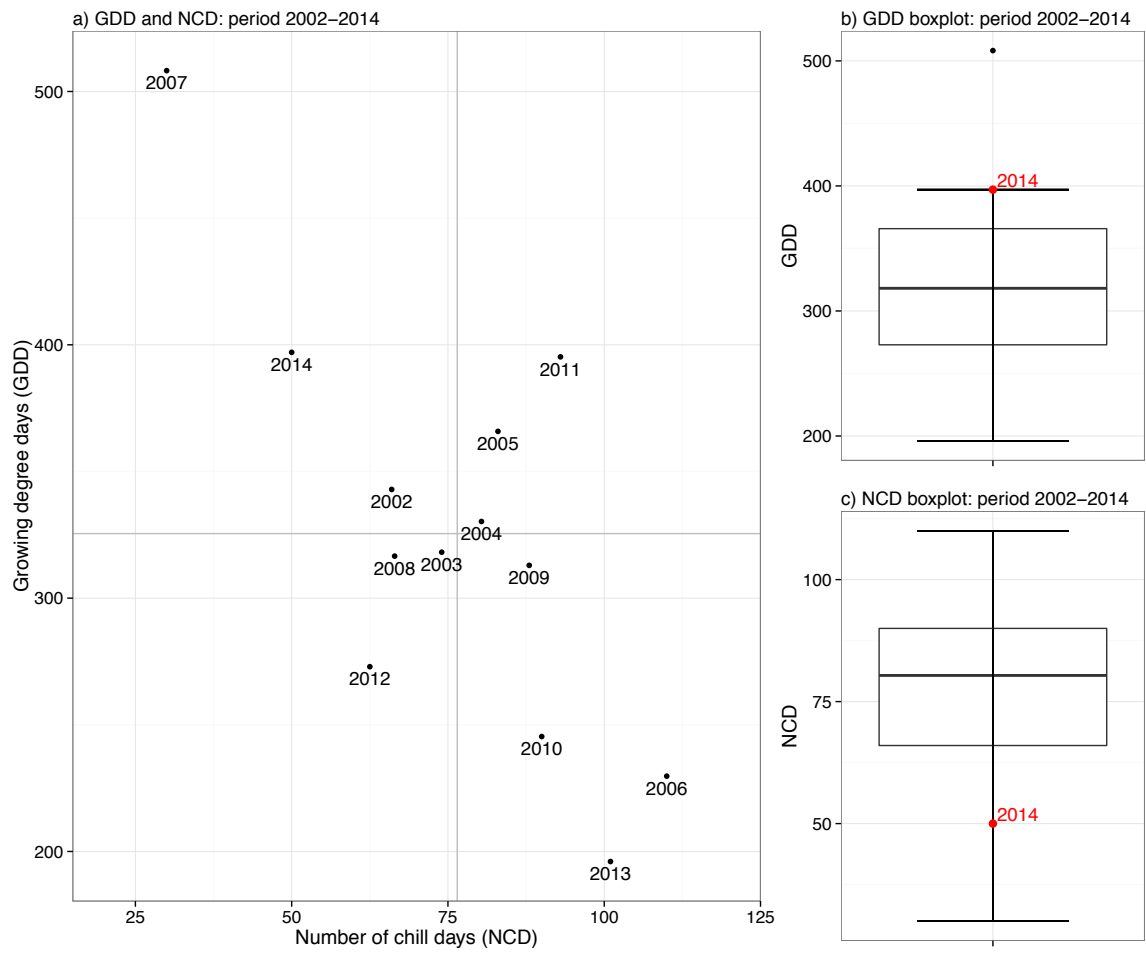


Figure 5.1.: Comparison of GDD and NCD for the years 2002-2014 (figure was first published in [Calders et al. \(2014a\)](#)).

## 6. Conclusion

In this research we compared low cost autonomous instruments with terrestrial lidar for spring phenology monitoring. We gathered a temporally dense dataset of terrestrial lidar and PASTIS57 data. We compared PASTIS57 derived plant area index (PAI) with TLS derived PAI. Logistic model fitting results were compared for the different data series. Start of season (SOS) was estimated from PAI data series and estimates were compared.

The most important result was that PASTIS57 could deliver PAI time series that stayed within a PAI range of 1 to TLS data. Fits of logistic models had a CV(RMSE) of 3.3%-5.8% for filtered PASTIS57 data and 1.5%-2.4% for TLS. Start of season (SOS) was estimated within 8 days of TLS derived SOS and varied 6 days at most with field observations.

PASTIS57 has been shown to be a cost-effective method for accurate large-scale phenology monitoring. It could be applied in monitoring campaigns measuring climate change induced phenology shifts.

Limitations found were that the sampling design of a PASTIS57 study needs to be well laid out. Many irradiance effects influence measurements. Proper positioning of instruments and their sensors in and outside of the forest can avoid such influences. Similarly, data processing needs to be laid out in an optimal way to derive the most accurate PAI values. Actual PAI values could not be measured using TLS and PASTIS57 instruments.

Further research should apply PASTIS57 in field campaigns where results can be validated and calibrated. Ground-truth PAI values could be acquired using a direct method. Phenological variables should be compared to regional phenology databases and air- and spaceborn sensor derived phenological time series. Research on PASTIS57 should focus on optimizing sampling design and data processing. Autonomous low cost instruments could fill a gap in available data acquiring techniques to make large-scale low cost longterm forest structure monitoring possible.

## Bibliography

- Baret, F., Lecerf, R., Mottus, M., and Rautinaen, M. PASTIS 57: Autonomous light sensors for PAI continuous monitoring. Principles, calibration and application to vegetation phenology. In *AGU Fall Meeting Abstracts*, number Figure 2, pages Abstract B52C-08, San Francisco, California, 2010.
- Bequet, R., Campioli, M., Kint, V., Vansteenkiste, D., Muys, B., and Ceulemans, R. Leaf area index development in temperate oak and beech forests is driven by stand characteristics and weather conditions. *Trees*, 25(5):935–946, May 2011. ISSN 0931-1890. doi: 10.1007/s00468-011-0568-4. URL <http://link.springer.com/10.1007/s00468-011-0568-4>.
- Black, T. A., Chen, W. J., Barr, A. G., Arain, M. A., Chen, Z., Nestic, Z., Hogg, E. H., Neumann, H. H., and Yang, P. C. Increased carbon sequestration by a boreal deciduous forest in years with a warm spring. *Geophysical Research Letters*, 27(9):1271–1274, 2000.
- Botta, A., Viovy, N., and Ciais, P. A global prognostic scheme of leaf onset using satellite data. *Global Change Biology*, 6:709–725, 2000. URL <http://onlinelibrary.wiley.com/doi/10.1046/j.1365-2486.2000.00362.x/abstract>.
- Calders, K., Verbesselt, J., Bartholomeus, H., and Herold, M. Applying terrestrial LiDAR to derive gap fraction distribution time series during bud break. In *Proceedings SilviLaser 2011, 11th international LiDAR forest applications conference, 16–20 Oct. 2011, Tasmania Hobart, Tasmania*, pages 1–9. University of Tasmania, 2011.
- Calders, K., Armston, J., Newnham, G., Herold, M., and Goodwin, N. Implications of sensor configuration and topography on vertical plant profiles derived from terrestrial LiDAR. *Agricultural and Forest Meteorology*, 194:104–117, 2014a.
- Calders, K., Schenkels, T., Bartholomeus, H., Armston, J., Verbesselt, J., and Herold, M. IN REVIEW: Monitoring spring phenology with high temporal resolution terrestrial LiDAR measurements. *Agricultural and Forest Meteorology*, 2014b.
- Che, M., Chen, B., Zhang, H., Fang, S., Xu, G., Lin, X., and Wang, Y. A New Equation for Deriving Vegetation Phenophase from Timeseries of Leaf Area Index (LAI) Data. *Remote Sensing*, 6(6):5650–5670, June 2014. ISSN 2072-4292. doi: 10.3390/rs6065650.
- Chiang, J.-M. and Brown, K. J. Improving the budburst phenology subroutine in the forest carbon model PnET. *Ecological Modelling*, 205(3-4):515–526, July 2007.

- ISSN 03043800. doi: 10.1016/j.ecolmodel.2007.03.013. URL <http://linkinghub.elsevier.com/retrieve/pii/S0304380007001470>.
- Culvenor, D. In-situ Sensing of Above-Ground Biomass in Support of National Biomass Mapping. Technical Report October, CSIRO Australia, Australia, 2012.
- Cutini, A., Matteucci, G., and Mugnozza, G. S. Estimation of leaf area index with the Li-Cor LAI 2000 in deciduous forests. pages 55–65, 1998.
- De Sy, V., Herold, M., Achard, F., Asner, G. P., Held, A., Kellndorfer, J., and Verbesselt, J. Synergies of multiple remote sensing data sources for REDD+ monitoring. *Current Opinion in Environmental Sustainability*, 4(6):696–706, Dec. 2012. ISSN 18773435. doi: 10.1016/j.cosust.2012.09.013. URL <http://linkinghub.elsevier.com/retrieve/pii/S1877343512001200>.
- Eitel, J. U., Vierling, L. a., and Magney, T. S. A lightweight, low cost autonomously operating terrestrial laser scanner for quantifying and monitoring ecosystem structural dynamics. *Agricultural and Forest Meteorology*, 180:86–96, Oct. 2013. ISSN 01681923. doi: 10.1016/j.agrformet.2013.05.012. URL <http://linkinghub.elsevier.com/retrieve/pii/S0168192313001561>.
- Gond, V., De Pury, D. G. G., Veroustraete, F., and Ceulemans, R. Seasonal variations in leaf area index, leaf chlorophyll, and water content; scaling-up to estimate fAPAR and carbon balance in a multilayer, multispecies temperate forest. *Tree physiology*, 19(10):673–679, Aug. 1999. ISSN 1758-4469.
- Herold, M. and Skutsch, M. Monitoring, reporting and verification for national REDD + programmes: two proposals. *Environmental Research Letters*, 6(1):014002, Jan. 2011. ISSN 1748-9326. doi: 10.1088/1748-9326/6/1/014002.
- Jeong, S.-J., Medvigy, D., Shevliakova, E., and Malyshev, S. Uncertainties in terrestrial carbon budgets related to spring phenology. *Journal of Geophysical Research*, 117(G1):G01030, Mar. 2012. ISSN 0148-0227. doi: 10.1029/2011JG001868. URL <http://doi.wiley.com/10.1029/2011JG001868>.
- Jonckheere, I., Fleck, S., Nackaerts, K., Muys, B., Coppin, P., Weiss, M., and Baret, F. Review of methods for in situ leaf area index determination. *Agricultural and Forest Meteorology*, 121(1-2):19–35, Jan. 2004. ISSN 01681923. doi: 10.1016/j.agrformet.2003.08.027. URL <http://linkinghub.elsevier.com/retrieve/pii/S0168192303001643>.
- Jonckheere, I., Nackaerts, K., Muys, B., and Coppin, P. Assessment of automatic gap fraction estimation of forests from digital hemispherical photography. *Agricultural and Forest Meteorology*, 132(1-2):96–114, Sept. 2005. ISSN 01681923. doi: 10.1016/j.agrformet.2005.06.003. URL <http://linkinghub.elsevier.com/retrieve/pii/S0168192305001152>.



- Jupp, D. L. B., Culvenor, D. S., Lovell, J. L., Newnham, G. J., Strahler, a. H., and Woodcock, C. E. Estimating forest LAI profiles and structural parameters using a ground-based laser called 'Echidna'. *Tree physiology*, 29(2):171–81, Mar. 2009. ISSN 0829-318X. doi: 10.1093/treephys/tpn022. URL <http://www.ncbi.nlm.nih.gov/pubmed/19203942>.
- Karlsen, S. R., Solheim, I., Beck, P. S. A., Hø gda, K. A., Wielgolaski, F. E., and Tø mmervik, H. Variability of the start of the growing season in Fennoscandia, 1982–2002. *International Journal of Biometeorology*, 51(6):513–524, 2007.
- Lovell, J., Haverd, V., Jupp, D., and Newnham, G. The Canopy Semi-analytic P gap And Radiative Transfer (CanSPART) model: Validation using ground based lidar. *Agricultural and Forest ...*, 158-159:1–12, 2012. ISSN 0168-1923. doi: 10.1016/j.agrformet.2012.01.020. URL <http://dx.doi.org/10.1016/j.agrformet.2012.01.020><http://www.sciencedirect.com/science/article/pii/S0168192312000512>.
- Melaas, E. K., Richardson, A. D., Friedl, M. A., Dragoni, D., Gough, C. M., Herbst, M., Montagnani, L., and Moors, E. Using FLUXNET data to improve models of springtime vegetation activity onset in forest ecosystems. *Agricultural and Forest Meteorology*, 171:46–56, 2013.
- Mussche, S., Samson, R., Nachtergale, L., Schrijver, A. D., Lemeur, R., and Lust, N. A Comparison of Optical and Direct Methods for Monitoring the Seasonal Dynamics of Leaf Area Index in Deciduous Forests. *Silva Fennica*, 35(October):373–384, 2001.
- Newnham, G., Armston, J., Muir, J., Goodwin, N., Culvenor, D., Püschel, P., Nys-tröm, M., and Johansen, K. Evaluation of Terrestrial Laser Scanners for Measuring Vegetation Structure, 2012.
- Rich, P. M. Characterizing plant canopies with hemispherical photographs. *Remote Sensing Reviews*, 5(1):13–29, Jan. 1990. ISSN 0275-7257. doi: 10.1080/02757259009532119. URL <http://www.tandfonline.com/doi/abs/10.1080/02757259009532119>.
- Richardson, A. D. and Keefe, J. O. Phenological differences between understory and overstory. In *Phenology of Ecosystem Processes*, pages 87–117. Springer, New York, NY, 2009. ISBN 978-1-4419-0025-8. doi: 10.1007/978-1-4419-0026-5. URL <http://link.springer.com/10.1007/978-1-4419-0026-5>.
- Ridler, T. and Calvard, S. Picture Thresholding Using an Iterative Selection Method. *IEEE transactions on Systems, Man ...*, (8):630–632, 1978.
- Ryu, Y., Lee, G., Jeon, S., Song, Y., and Kimm, H. Monitoring multi-layer canopy spring phenology of temperate deciduous and evergreen forests using low-cost spectral sensors. *Remote Sensing of Environment*, 149:227–238, June 2014. ISSN 00344257. doi: 10.1016/j.rse.2014.04.015. URL <http://linkinghub.elsevier.com/retrieve/pii/S0034425714001588>.

- Schleppi, P., Conedera, M., Sedivy, I., and Thimonier, A. Correcting non-linearity and slope effects in the estimation of the leaf area index of forests from hemispherical photographs. *Agricultural and Forest Meteorology*, 144(3-4):236–242, June 2007. ISSN 01681923. doi: 10.1016/j.agrformet.2007.02.004. URL <http://linkinghub.elsevier.com/retrieve/pii/S0168192307000640>.
- Simic, A., Baret, F., Weiss, M., Lecerf, R., Alessandrini, A., Hanocq, J.-F., and Marloie, O. Production of the high resolution maps of biophysical variables based on SPOT imagery and in-situ measurements generated by PASTIS 57 for Hyytiala, Finland. In *Geoscience and Remote Sensing Symposium (IGARSS), 2012 IEEE International*, pages 7655–7658. IEEE, 2012.
- Vitasse, Y., Delzon, S., Dufrêne, E., Pontailleur, J.-Y., Louvet, J.-M., Kremer, A., and Michalet, R. Leaf phenology sensitivity to temperature in European trees: Do within-species populations exhibit similar responses? *Agricultural and Forest Meteorology*, 149(5):735–744, May 2009. ISSN 01681923. doi: 10.1016/j.agrformet.2008.10.019. URL <http://linkinghub.elsevier.com/retrieve/pii/S0168192308003055>.
- Von Wuehlisch, G., Krusche, D., and Muhs, H. J. Variation in temperature sum requirement for flushing of beech provenances. *Silvae Genetica*, 44:343–345, 1996.
- Waring, R. H. and Running, S. W. *Forest ecosystems: analysis at multiple scales*. Elsevier, 2010.
- WMO. *Guide to Climatological Practices WMO-No. 100 (third edition)*. Number 100. 2011. ISBN 9789263101006.
- Zhao, F., Yang, X., Schull, M. a., Román-Colón, M. O., Yao, T., Wang, Z., Zhang, Q., Jupp, D. L. B., Lovell, J. L., Culvenor, D. S., Newnham, G. J., Richardson, A. D., Ni-Meister, W., Schaaf, C. L., Woodcock, C. E., and Strahler, A. H. Measuring effective leaf area index, foliage profile, and stand height in New England forest stands using a full-waveform ground-based lidar. *Remote Sensing of Environment*, 115(11): 2954–2964, Nov. 2011. ISSN 00344257. doi: 10.1016/j.rse.2010.08.030. URL <http://linkinghub.elsevier.com/retrieve/pii/S0034425711001416>.

# A. Fieldwork Guidelines Dassenbos 2014

## Introduction

Four plots (A – B – C – D) are established in Dassenbos. The objective is to measure budburst with a range of different sensor. First measurements were done on 24 Feb 2014. The intention is to revisit the plots every Mon/Wed/Fri. Data is stored on the bananas lidar-computer (office C207).

## Overview sensors

1. TLS
2. HP with DSLR
3. HP with smartphone
4. PASTIS57

## Measurement protocol

Visit plot A first, then B, C and D.

### Terrestrial LiDAR

1. Set up tripod at 1.45m
2. Put scanner on tripod with screw number 1.
3. Orient the y-axis towards North ( $270^{\circ}$  on scanner mount).
4. Adjust tripod position so that plummet laser is above small wooden pole
5. Adjust the camera settings to light conditions
6. Make new riscan project
7. First scan = upright = ScanPos001. Pattern = 006centre
8. Second scan = tilted 90deg = ScanPos002. Pattern = 006hemi
9. Make a new riscan project for each plot

### **Hemispherical photos with DSLR**

1. Camera should have correct settings already:
  - a) Aperture priority (A) with F-stop fixed at 2.8, ISO 400
  - b) Bracketing enabled to take 3 pictures (with normal exposure, one under, one over).
  - c) Have the “lower wheel” on C1 so you can hold button and take 3 pics in one go.
2. Tripod height at 1.3m. Level bulb oriented towards North.
3. Bracketing is enabled. Take the 3 pictures.

### **Hemispherical photos with smartphone**

1. Make 1 photo per plot.

## B. Hemispherical photography

Hemispherical photographs were gathered during the field campaign. PAI values derived from them never gave a valid PAI time series. We have included our approach in this appendix for possible future investigation.

### B.1. Introduction

Hemispherical photographs were gathered during the field campaign to provide another PAI time series next to TLS for comparison. This method is often employed for PAI measurements [Jonckheere et al. \(2004\)](#). Optimal estimations can only be derived when photographs are made with even light conditions. During our field campaign this was not the priority because TLS measurements can be made under any light conditions. Therefore hemispherical photographs were often gathered in sub-optimal light conditions.

### B.2. Methods

Digital hemispherical photographs were made using a Nikon D7000 camera with a Sigma 4.5mm F2.8 lens. The camera was set to aperture priority, F-stop fixed to 2.8, ISO set to 400, Autofocus, bracketing is set to take 3 pictures (one with normal exposure, one underexposed, one overexposed). The camera is positioned on a tripod so that the top of the lens is 1.4m from the ground. The camera is oriented towards the canopy with the top pointing North. It was then leveled using a leveling bulb attached to the camera. Three photographs were made and checked for proper focusing.

Photos were made at the four field plots every monday, wednesday and friday throughout the whole campaign. Because of the fixed schedule occasionally photos were made under sub-optimal weather conditions.

A manual selection of photographs was made to correct for exposure differences between measurements. Images containing sun flare were excluded. This made for gaps in the time series with a maximum length of eight days.

Photos were processed using the Hemisfer software package (Swiss Federal Institute for Forest, Snow and Landscape Research WSL). Analysis was done for 14 rings of  $5^\circ$ , thus the  $0-70^\circ$  zenith angle range was used. Only the blue band is used because it shows most contrast between vegetation and sky ([Zhao et al., 2011](#)). Gamma correction is set to 2.2. The [Ridler and Calvard \(1978\)](#) method was used for the tresholding process. This method was shown to produce most accurate and robust results for a wide range of situations in [Jonckheere et al. \(2005\)](#). Norman & Campbell and Chen & Cihlar (with  $p = 0.02$ ) methods are applied as in [Schleppi et al. \(2007\)](#) and [Calders et al. \(2011\)](#).

### B.3. Results

PAI time series acquired using hemispherical photography is shown in Fig. B.1. PAI values often vary more than 1 between subsequent measurements. PAI values range from about 0 to 2.5-3 during the field campaign. A PAI increase of about 1.0 to 2.0 seems to be present from DOY 100 to 130.

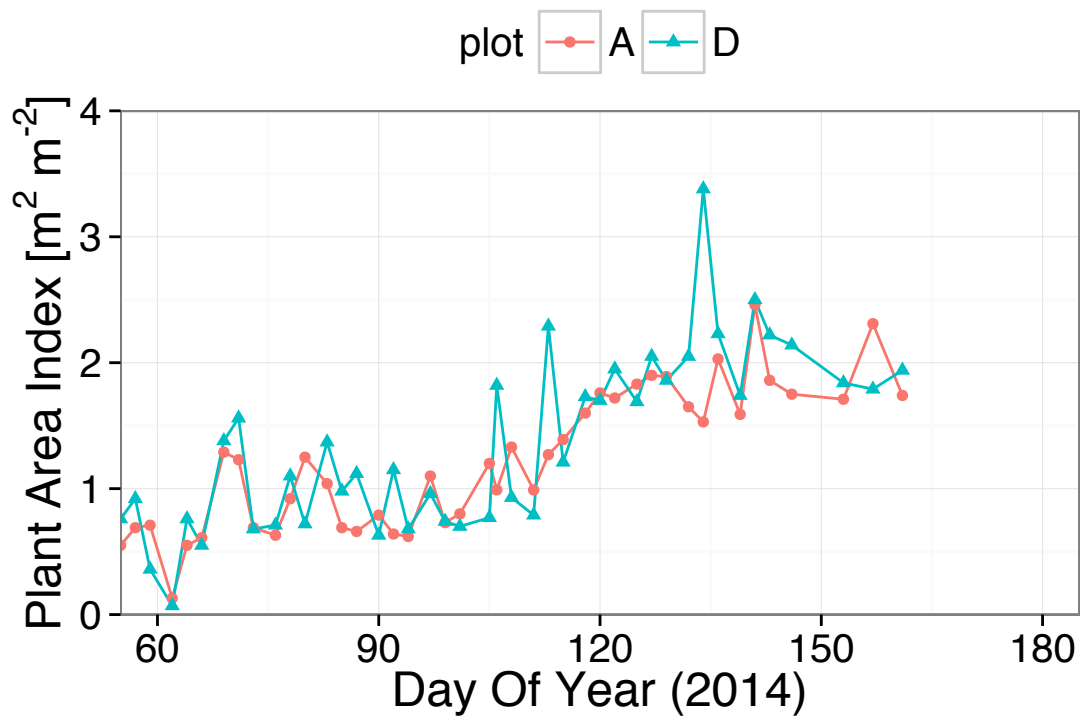


Figure B.1.: PAI time series derived from hemispherical photography for plot A and D.

### B.4. Discussion

PAI variations like these are something unexpected which we did not see in literature (Mussche et al., 2001). The variance could be caused by sub-optimal weather conditions during data gathering. Many photographs contain both direct sunlight and clouds. But not all photographs are influenced like this, so we expected more PAI estimates in the same range as the other data series. The precise factors leading to the large variation in PAI were not determined.

PAI estimations from hemispherical photographs are lower than PASTIS57 and TLS estimates by at least 1. This difference might partially be caused by the underestimation known for passive instruments as described in Section 5.

## C. R script listings

**processP57.R** Process PASTIS57 csv files into daily PAI measurements

```
1 # Derive daily PAI values and save to plot
2 # by Tom Schenkels
3
4 setwd("/Users/tom/Dropbox/Studie/Thesis/Projects/")
5 source("inc/frontmatter.R")
6 removeSuperfluousData = TRUE
7
8 # readP57file(fname string filename): data frame with timesynced,
9 readP57file <- function(fname){
10 # Supply english names for columns
11   columnNames = c("datetime", "ID", "V1", "V2", "V3", "V4", "V5",
12     "V6", "Temp.")
13
14 # Read csv, apply english column names
14   df = read.csv(
15     sep=";",
16     header=FALSE,
17     skip=10,
18     col.names=columnNames,
19     as.is=c(1),
20     fname)
21
22 # Add rounded off time variable Datetime
23 posixDatetime = as.POSIXct(df$datetime,format="%d/%m/%Y - %X")
24 df$DateTimes <-as.POSIXct(round(as.double(posixDatetime)/(5*60))
25   *(5*60),origin=(as.POSIXlt('1970-01-01')))
26
27 # Remove data before 27-2
27   df = df[df$DateTimes >= as.POSIXct("2014-02-27 00:00"),]
28
29 # Remove unnecessary columns
30   if(removeSuperfluousData){
31     df = df[, !(names(df) %in% c("datetime", "Temp.", "ID"))]
32   }
33   return(df)
34 }
35
36 # Read A-D and o1 csv files
37 #####
```

```

38
39 # PASTIS NUMBERS IN DASSENBOSS:
40 # "OUTSIDE FOREST" SENSORS:
41 # 213 orientations
42 # & 211 (211 replaced by 209 on 22 April 2014)
43 # PLOT A: 227,
44 # PLOT B: 240
45 # PLOT C: 188
46 # PLOT D: 190
47
48 P57_C = readP57file("PAI/PASTIS57/Data/188_140702_1102.csv")
49 P57_D = readP57file("PAI/PASTIS57/Data/190_140702_1105.csv")
50
51 #P57_o2B = readP57file("Data/209_140514_1008.csv")
52 #P57_o2A = readP57file("Data/211_140422_1400.csv")
53 #P57_o2 = merge(sort=FALSE, all.x=TRUE, all.y=TRUE, P57_o2A, P57_
o2B)
54 P57_o1 = readP57file("PAI/PASTIS57/Data/213_140702_1125.csv")
55
56 P57_A = readP57file("PAI/PASTIS57/Data/227_140702_1053.csv")
57 P57_B = readP57file("PAI/PASTIS57/Data/240_140702_1057.csv")
58
59 nRemoved = as.numeric(c())
60
61 #####
62 # f: calculates PAIs for a plot, prints plot to output and returns
data.
63 # :df(daily;doy and PAI stats, complete;complete PAI calculations)
64 #####
65 derivePAI = function(dfOpen, dfClosed,
66 openWiresToRemove, closedWiresToRemove,
67 plotname){
68 ##### PLOT doy vs PAI median, 95% bars
69 # sync open & closed instrument dataframes
70 P57_oXc = merge(dfOpen, dfClosed, by="DateTimeS")
71
72 # remove wrong wires from both (5&6 for open site, dynamic for
closed site)
73 all = 1:length(P57_oXc)
74 drops = append(openWiresToRemove + 1, closedWiresToRemove + 7)
75 keeps = all[! all %in% drops]
76 P57_oXc = P57_oXc[, keeps, drop=FALSE]
77 names(P57_oXc) = "DateTimeS"
78 rm(all,drops,keeps, closedWiresToRemove, openWiresToRemove)
79
80 # filter 4079 values (check a good amount is removed)
81 for(i in 2:9) P57_oXc = P57_oXc[ P57_oXc[i] < 4000, ]
82
83 # apply averaging for open site and closed site values

```



```

84 P57_oXc['avg_o'] = apply(P57_oXc[,2:5], 1, mean)
85 P57_oXc['avg_c'] = apply(P57_oXc[,6:9], 1, mean)
86
87 # apply PAI = -cos(HA)/G(HA)*log(transmitted/incident) = -1.075*
      log(transmitted/incident)
88 P57_oXc['PAI'] = -1.075*log(P57_oXc$avg_c/P57_oXc$avg_o)
89 # remove <= 0 and infinite values
90 P57_oXc = do.call(data.frame, lapply(P57_oXc, function(x)
      replace(x, x<=0| is.infinite(x),NA)))
91 P57_oXc["doy"] = as.numeric(strftime(P57_oXc$DateTimes, format="
      %j"))
92
93 # add daily mean and median values by looping over days
94 doym = vector(); mean = vector(); sd = vector(); median = vector
      (); q25 = vector(); q75 = vector();
95 for(i in unique(P57_oXc$doy)) {
96   doym = append(doym, i)
97   # get day PAI values without 0, Inf & NAs
98   dailyPAIs = P57_oXc[P57_oXc$doy==i & !is.na(P57_oXc$PAI) & is.
      finite(P57_oXc$PAI), 'PAI']
99   mean = append(mean, mean(dailyPAIs))
100  sd = append(sd, sd(dailyPAIs))
101  median = append(median, median(dailyPAIs))
102  q25 = append(q25, quantile(dailyPAIs, c(.25), na.rm = TRUE)
      [[1]])
103  q75 = append(q75, quantile(dailyPAIs, c(.75), na.rm = TRUE)
      [[1]])
104 }
105 P57_oXc_doy = data.frame(doym, mean, sd, median, q25, q75)
106 rm (i, dailyPAIs, doym, mean, sd, median, q25, q75)
107
108 qplot(doym, median, data=P57_oXc_doy, geom = c("point"))+
109   geom_smooth(aes(y=median)) # span=1
110
111 return(list(daily = P57_oXc_doy, complete = P57_oXc))
112 }
113
114 A = derivePAI(P57_o1, P57_A, c(5,6), c(5,6))
115 B = derivePAI(P57_o1, P57_B, c(3,4), c(3,4))
116 C = derivePAI(P57_o1, P57_C, c(5,6), c(5,6))
117 D = derivePAI(P57_o1, P57_D, c(5,6), c(5,6))
118
119 # Add plot letters to daily dataframes
120 A$daily['plot'] = as.factor("A")
121 B$daily['plot'] = as.factor("B")
122 C$daily['plot'] = as.factor("C")
123 D$daily['plot'] = as.factor("D")
124
125 # remove bad days: DOY 175-176 for moving and DOY183 for Nepal

```

```

      time
126 A$daily = A$daily[
127   A$daily$doy != 175&
128   A$daily$doy != 176&
129   A$daily$doy != 183,]
130 B$daily = B$daily[
131   B$daily$doy != 175&
132   B$daily$doy != 176&
133   B$daily$doy != 183,]
134 C$daily = C$daily[
135   C$daily$doy != 175&
136   C$daily$doy != 176&
137   C$daily$doy != 183,]
138 D$daily = D$daily[
139   D$daily$doy != 175&
140   D$daily$doy != 176&
141   D$daily$doy != 183,]

```

### **filterP57.R** Filter PASTIS57 data using sunshine hours

```

1  setwd("/Users/tom/Dropbox/Studie/Thesis/Projects/")
2  source("inc/frontmatter.R")
3
4  # Set filenames
5  P57File = "PAI/Output/2014-07-15_20.42_PAI_P57.csv"
6  sunlightFile = "Meteo/weather_summary_10min.txt"
7
8  # Get P57 data ready
9  P57 = read.csv(P57File, header = TRUE)
10 P57 = P57[P57$method == "",2:6]
11 P57$type = as.factor("PAI [m2-1 m2]")
12
13 # Get sunlight data ready
14 sunlight = read.table(sunlightFile, header = TRUE)
15 doy = sunlight$DOY
16 sunlight_hours = sunlight$cumulative_daily_sunlight_.hours.
17 sunlight = data.frame(DOY = doy, instrument="", plot="", method=""
18   , PAI = sunlight_hours, type = "daily sunlight hours [h]")
18 rm(doy, sunlight_hours)
19 sunlight = sunlight[sunlight$DOY >= 58, ]
20
21 # Determine dark days with a low amount of sunlight
22 darkdays = sunlight[sunlight$PAI < 4, 1]
23
24 # Plot data with darkday plotted
25 p = qplot(DOY, PAI, data=rbind(P57, sunlight), geom = c("line"),
26   color=plot)
27 p = p + facet_grid(type ~ ., scales="free")
28 p = p + ylab("PAI and sunlight hours")

```

```

29 p = p + geom_vline(xintercept = darkdoys, alpha = .5)
30 p
31
32 # Remove darkday data and save csv
33 P57_sundays = P57[!P57$DOY %in% darkdoys,] # remove darkdoys from
    P57
34 P57_sundays$method = "filtered >5h sunlight"
35 P57_sundays$type = as.factor("PAI [m2-1 m2]'"")
36 #save.data("PAI_P57_5-sun-hours", P57_sundays[,1:5])

```

### sigmoids.R Fit logistical models to PASTIS57 measurements

```

1 # Fit sigmoids for PASTIS57 data
2 # by Tom Schenkels
3
4 setwd("/Users/tom/Dropbox/Studie/Thesis/Projects/")
5 source("inc/frontmatter.R")
6
7 # Set filenames
8 # HPfile = "PAI/Output/2014-07-01_16.43_PAI_HP.csv"
9 P57file = "PAI/Output/2014-07-15_20.42_PAI_P57.csv"
10 P57sfile = "PAI/Output/2014-07-22_00.15_PAI_P57_5-sun-hours.csv" #
    use only sunny day data (>5 hours)
11 # TLSfile = "PAI/Output/2014-07-09_11.05_PAI_TLS.csv"
12 paiFileName = "PAIA11"
13
14 # Read
15 # HP = read.csv(HPfile)
16 P57 = read.csv(P57file)
17 P57s = read.csv(P57sfile)
18 # TLS = read.csv(TLSfile)
19 # data = rbind(HP, P57, P57s, TLS)
20 data = rbind(P57, P57s)
21
22 data$label = sprintf("%s plot %s %s", data$instrument, data$plot,
    data$method)
23 unique(data$label)
24
25
26
27 ##### ESTABLISH SIGMOID FUNCTIONS
28 {
29 # function needed for visualization purposes
30 sigmoid = function(params, x) {
31     params[4] + ((params[1] - params[4]) / (1 + exp(-params[2] * (x -
        params[3] ))))
32 }
33
34 sigmoid_deriv=function(params, x) {

```

```

35     (params [2] * (params [1]-params [4]) * exp(params [2] * (params
      [3] + x)))/(exp(params [2]*params [3])+exp(params [2]*x))^2
36   }
37
38   sigmoid_deriv2=function(params , x) {
39     (params [2]^2*(params [1]-params [4])*exp(params [2])*(params [3]+x
      )*(exp(params [2]*params [3])-exp(params [2]*x)))/(exp(params
      [2]*params [3])+exp(params [2]*x))^3
40   }
41
42   fitModel = function(df){
43     x = df$DOY
44     y = df$PAI
45     fitModel = nls(y ~ d +((a-d) / (1 + exp(-b * (x - c))))), trace
      =FALSE,start = list(a = 4.5, b = 0.1, c = 100,d=2))
46     params = coef(fitModel)
47     df$y2 = sigmoid(params , x)
48     y2<-df$y2
49     df$y3 = sigmoid_deriv(params , x)
50     y3<-df$y3
51     df$y4 = sigmoid_deriv2(params , x)
52     y4<-df$y4
53
54     m<-fitModel
55     RMSE=round(sqrt(mean(residuals(m)^2)), digits=2)
56     CVRMSE=round(RMSE/mean(df$PAI),3)*100
57     confint = signif(confint(fitModel),4)
58     ULLA = max(confint [4,])
59     SOS = x[which(df$y2 > ULLA)[1]]
60     # alternative method using ratio of difference to get SOS
      border
61     LAL = (params [1]-params [4])/75
62     SOS2 = x[which(df$y2 > params [4]+LAL)[1]]
63
64
65     print(paste("CVRMSE", CVRMSE))
66
67     print("U,      k,      tm,      L")
68     print(signif(params ,4))
69     print(t(confint []))
70
71     print(
72       paste(
73         "U-L",
74         round(params [1]-params [4],2)
75       )
76     )
77
78     print(paste("SOS", SOS))

```

```

79     print(paste("SOS2", SOS2))
80
81     return(df)
82 }
83 }
84
85
86 ##### DERIVE SIGMOIDS
87 P57_A_complete_sigmoid = fitModel(P57[P57$plot=="A" & P57$method
   =="" ,])
88 P57_A_filtered_sigmoid = fitModel(P57s[P57s$plot=="A" ,])
89
90 P57_B_complete_sigmoid = fitModel(P57[P57$plot=="B" & P57$method
   =="" ,])
91 P57_B_filtered_sigmoid = fitModel(P57s[P57s$plot=="B" ,])
92 P57_C_complete_sigmoid = fitModel(P57[P57$plot=="C" & P57$method
   =="" ,])
93 P57_C_filtered_sigmoid = fitModel(P57s[P57s$plot=="C" ,])
94 P57_D_complete_sigmoid = fitModel(P57[P57$plot=="D" & P57$method
   =="" ,])
95 P57_D_filtered_sigmoid = fitModel(P57s[P57s$plot=="D" ,])

```

#### 01runModel.R Run NCD-GDD model on meteo data 2013-2014

```

1 ## Kim Calders, Tom Schenkels - May 2014
2 source("/Users/tom/Dropbox/Studie/Thesis/Projects/inc/frontmatter.
   R")
3
4 NCD=22
5 GDD=0
6
7 a = -68; b = 638; c = -0.01 # jeong2012uncertainties
8
9 outfile <- file('weather_station/GDD.txt', 'w') #make a space
   seperated output file
10 writeLines(paste("DOY","Tmax","Tmin","GDD","NCD","f"), con=outfile
   ) #write header
11 con_in=file("weather_station/doy_in.txt",open="r")
12 while (length(oneLine <- readLines(con_in, n = 1, warn = FALSE)) >
   0) { #this reads the input file line by line
13
14     if (.Platform$OS.type == "windows") {
15         inFile <- paste("data_doy\\",oneLine, ".txt",sep="")
16     } else {
17         inFile <- paste("weather_station/data_doy/",oneLine, ".txt",sep
   = "")
18     }
19
20     data <- read.csv(inFile, header=F)

```

```

21 DOY=as.integer(oneLine)
22
23 #calculate
24 maxT=round(max(data$V5),2)
25 minT=round(min(data$V4),2)
26 avgT=mean(data$V3) #TS
27 #avgT=(maxT+minT)/2 #KC
28 baseT=5 #Bequet et al
29
30
31 dayGDD=avgT-baseT
32 if (dayGDD<0) {dayGDD=0}
33 GDD = GDD + dayGDD
34
35 if (avgT<5) {NCD=NCD+1}
36
37 f = a + b * exp(c*NCD)
38
39 #APPEND THESE TO A NEW MATRIX
40 writeLines(paste(DOY,maxT,minT,GDD,NCD,f), con=outfile)
41
42 }
43 close(con_in)
44 close(outfile)

```